Journal of Power Sources 251 (2014) 379–385

Contents lists available at ScienceDirect

Journal of Power Sources

journal homepage: www.elsevier.com/locate/jpowsour

Short communication

Anatase TiO_2 nanoparticles for high power sodium-ion anodes

Liming Wu, Daniel Buchholz, Dominic Bresser*, Luciana Gomes Chagas, Stefano Passerini*

Institute of Physical Chemistry & MEET Battery Research Centre, University of Muenster, Corrensstrasse 28/30 & 46, 48149 Muenster, Germany

HIGHLIGHTS

- Anatase TiO_2 nanoparticles reveal reversible Na-ion uptake and release.
- Effect of electrolyte composition on cyclability of anatase TiO_2 Na-ion anodes.
- Anatase TiO_2 electrodes show superior high rate capability.
- Anatase TiO_2 electrodes offer extremely long cycle life at elevated C rates.

ARTICLE INFO

Article history:
Received 18 October 2013
Received in revised form
22 November 2013
Accepted 23 November 2013
Available online 7 December 2013

Keywords:
Anatase TiO_2 nanoparticles
Anode
High power
Electrolyte
Sodium-ion battery

ABSTRACT

Sodium-ion batteries (SIBs) are considered to be a promising low-cost alternative to common lithium-ion batteries. Herein, we present a detailed electrochemical characterization of anatase TiO_2 nanoparticles as anode material for Na-ion batteries, highlighting the substantial influence of the electrolyte composition (salt and solvent) on the obtainable specific capacity, cycling stability, and particularly the coulombic efficiency. TiO_2-based electrodes cycled using a 1M solution of $NaClO_4$ in a mixture of ethylene carbonate and propylene carbonate present excellent high rate capability, offering about 100 and 86 mAh g^{-1} at 5.5 and 11C, respectively, which is – to the best of our knowledge – the best high rate capability for all titanium-based sodium-ion anode materials reported so far. Setting the C rate to 5.5C (*i.e.*, 1.85 A g^{-1}), such electrodes can be cycled for more than 1000 cycles without significant capacity decay, confirming their outstanding durability at such high specific current. These results, in combination with its environmental friendliness and cost efficiency, render anatase TiO_2 nanoparticles a promising anode material for high power sodium-ion batteries.

1. Introduction

State-of-the-art lithium-ion batteries are nowadays dominating the market for portable electronic devices due to their efficient energy storage, advanced cycling stability, and, in particular, high energy and power densities [1,2]. Accordingly, they are considered as most promising battery technology for large-scale applications, such as electric vehicles and stationary energy storage [3,4]. However, considering the long-term view in which the whole transportation sector might be fully electric, powered by lithium-based batteries, this might raise concerns about its availability, particularly because of its inhomogeneous distribution within the Earth's crust [5,6]. Thus, especially for stationary energy storage applications, for which the weight and volume of a battery are less critical factors but cost is of major importance, alternative battery technologies are currently under evaluation. One of these, gathering rapidly increasing interest by research groups all around the world, is the sodium-ion battery. In general, sodium is a uniformly distributed and abundant element, providing the great chance of very cost-efficient and environmentally friendly electrochemical energy storage devices. Moreover, this technology offers the advantage that several research and development stages can be leapfrogged and scientific knowledge gained in the field of lithium-ion batteries can be frequently adopted. In fact, a huge variety of suitable high performance cathode materials was already identified and developed within recent years [7–10]. *Inter alia*, layered transition metal oxides [11–13], polyanionic compounds [14], and NASICON-type sodium metal phosphates [15,16] were studied and showed promising electrochemical performance.

With respect to the anode side, however, only few materials were reported so far. Graphite, the state-of-the-art anode material for lithium-ion batteries, unfortunately, can host only very little if any sodium ions by intercalation [17]. Instead, hard carbons appear to show a more appealing sodium storage capability [18–20]. Nevertheless, the generally rather low operational potential raises

* Corresponding authors. Tel.: +49 251 8336725; fax: +49 2518336797.
E-mail addresses: dominic.bresser@uni-muenster.de (D. Bresser), stefano.passerini@uni-muenster.de (S. Passerini).

0378-7753/$ – see front matter © 2013 Elsevier B.V. All rights reserved.
http://dx.doi.org/10.1016/j.jpowsour.2013.11.083

severe safety issues for practical applications, as for instance, metallic sodium plating and sodium dendrite formation. Beside (inter)metallic compounds, such as Sn [21–25], Cu_6Sn_5 [26], Sb [27], or NiP_3 [28], recently also classical insertion materials as, for instance, sodium titanates ($Na_2Ti_3O_7$) were proposed as an alternative anode material, operating at a slightly elevated potential of around 0.3 V *vs.* Na/Na^+ [29–32]. Very recently also TiO_2 (B) was studied as alternative sodium-ion anode material [33]. However, such a material showed only a rather low specific capacity of about 80 mAh g^{-1} for an applied specific current of 50 mA g^{-1}, which was further decreasing to about 35 mAh g^{-1} at 400 mA g^{-1}. Finally, beside sodium titanates and TiO_2 (B) also amorphous TiO_2 nanostructures were investigated with respect to its suitability as sodium-ion host material [34–36].

Regarding anatase TiO_2, initially only some preliminary studies were performed. Kavan et al. [37] investigated the formation of an accumulation layer on nanocrystalline anatase TiO_2, comparing *inter alia* sodium and lithium, concluding that no reversible sodium insertion into the anatase lattice took place using their experimental setup. A basically theoretical study, however, showed that the activation barrier for sodium insertion into the anatase lattice would be comparable to that for lithium, which is rather remarkable considering its significantly larger radius [38]. Very recently, Xu et al. [39] reported for the first time the application of nanocrystalline anatase TiO_2, synthesized by using cellulose-based paper as sacrificial template and titanium isopropoxide as precursor, as sodium-ion anode material. The presented electrochemical performance of electrodes based on this active material and poly(vinylidene difluoride) as binder (about 150, 70, and 50 mAh g^{-1} at specific currents of 50, 1000, and 2000 mA g^{-1}) is certainly very promising and encourages further studies on this new sodium-ion anode material.

Herein, we present a detailed electrochemical study on the utilization of commercial nanoparticulate anatase TiO_2 as active material for sodium-ion anodes using environmentally friendly sodium carboxymethyl cellulose as binder. Such electrodes were characterized by means of cyclic voltammetry and galvanostatic cycling at constant and elevated C rates. Remarkably, the observed electrochemical performance is strongly dependent on the utilized electrolyte composition. Thus, three different sodium salts ($NaClO_4$, $NaPF_6$, and NaTFSI) and three solvents or solvent mixtures (PC; EC:PC, 1:1; and EC:DMC, 1:1) were studied, revealing that stable cycling at high specific capacities and high coulombic efficiencies are only possible for carefully selected combinations of salt and solvent.

2. Experimental section

The structure and morphology of anatase TiO_2 nanoparticles (SIGMA ALDRICH, used as received) was investigated by means of X-ray diffraction (XRD, BRUKER D8 Advance; Cu-Kα radiation, λ = 0.154 nm) and scanning electron microscopy (SEM, ZEISS Auriga®). The Brunauer–Emmett–Teller (BET) surface area was determined by nitrogen adsorption measurements using an ASAP 2020 (Accelerated Surface Area and Porosimetry Analyzer, MICROMERITICS).

For the electrochemical characterization, electrodes were prepared having a final composition of 70 wt.% anatase TiO_2, 20 wt.% conductive carbon (SuperC65®, TIMCAL) and 10 wt.% sodium carboxymethyl cellulose (CMC, WALOCEL™CRT 2000 PPA 12, Dow Wolff Cellulosics). First, CMC was dissolved in deionized water to obtain a 1.25 wt.% solution. Subsequently, the conductive carbon and TiO_2 nanoparticles were added and the resulting mixture was dispersed by ball milling for 3 h. The obtained slurry was then casted on dendritic copper foil (SCHLENK). After drying at room temperature, disk electrodes (Ø = 12 mm) were punched and dried for 20 h at 120 °C under vacuum. The active material mass loading of the so-obtained electrodes was between 1.4 and 1.6 mg cm^{-2}. Three-electrode Swagelok™ cells were assembled in an MBraun glove box with an oxygen and water content below 0.5 ppm. Sodium metal (99.8%, ACROS ORGANICS) was used as counter and reference electrode. Thus, all potential values given in this manuscript refer to the Na/Na^+ reference couple. For the evaluation of different electrolyte compositions the following sodium salts and solvents were used as received: $NaPF_6$ (98%, SIGMA ALDRICH), NaTFSI (99.5%, SOLVIONIC), $NaClO_4$ (98% SIGMA ALDRICH), propylene carbonate (PC, SIGMA ALDRICH), ethylene carbonate (EC, UBE) and dimethyl carbonate (DMC, UBE). A sheet of Whatman™ glass fiber was used as separator.

Galvanostatic cycling and cyclic voltammetry were carried out utilizing a Maccor Battery Tester 4300 and a VMP3 Potentiostat (BIOLOGIC), respectively. All electrochemical studies were performed at ambient temperature (20 ± 2 °C). Considering the reversible uptake of one sodium ion per formula unit of TiO_2 the theoretical specific capacity would be 335 mAh g^{-1}. Accordingly, we defined an applied specific current of 335 mA g^{-1} as a C rate of 1C.

3. Results and discussion

3.1. Structural and morphological characterization

Prior to the electrochemical characterization, XRD and SEM analysis of the anatase TiO_2 nanoparticles was performed. XRD analysis revealed that the purchased sample was indeed purely anatase (space group $I4_1/amd$, JCPDS reference no. 00-021-1272) and no additional reflections, indicating possible phase impurities, were observed (Fig. 1a). In Fig. 1b a SEM image of the nanoparticulate TiO_2 is presented, showing that the particles have a rather uniform size distribution, almost spherical shape, and average diameter of around 30 nm. This is in rather good agreement with the determined BET surface area of about 45.1 m^2 g^{-1}, confirming the small particles size according to a rough calculation assuming perfectly spherical particles (Ø particle diameter = 2 * (3/BET surface area/density) * 1000 ≈ 34 nm; density (anatase TiO_2) = 3.89 g cm^{-3}). SEM images of the subsequently prepared electrodes at different magnifications are presented in Fig. 1c and d, showing the rather porous morphology of the coating layer and a homogenous distribution of the nanosized particles, revealing that the active material was well dispersed upon electrode preparation. Nevertheless, a clear distinction between the TiO_2 nanoparticles and the conductive carbon nanoparticles is not that simple due to the similar particle size of the two.

3.2. The influence of the electrolyte

The careful selection of a suitable electrolyte composition is certainly essential for optimizing the electrochemical performance of any active material utilized in sodium-ion batteries [40,41]. Generally, propylene carbonate (PC) is a very attractive electrolyte solvent due to its high dielectric constant and wide liquidus range [40], particularly, since the reversible alkali metal ion uptake and release in anatase TiO_2 does not mandatorily require the formation of a suitable solid electrolyte interphase (SEI). Thus, we focused initially on PC as electrolyte solvent while varying the conductive salt ($NaClO_4$, $NaPF_6$, and NaTFSI). For a detailed characterization of the electrolyte characteristics (*i.e.*, its conductivity, viscosity, thermal and electrochemical stability) the interested reader is referred to a very recent study reported by Palacin and co-workers [41]. The reversible sodium ion storage in anatase TiO_2 using the different

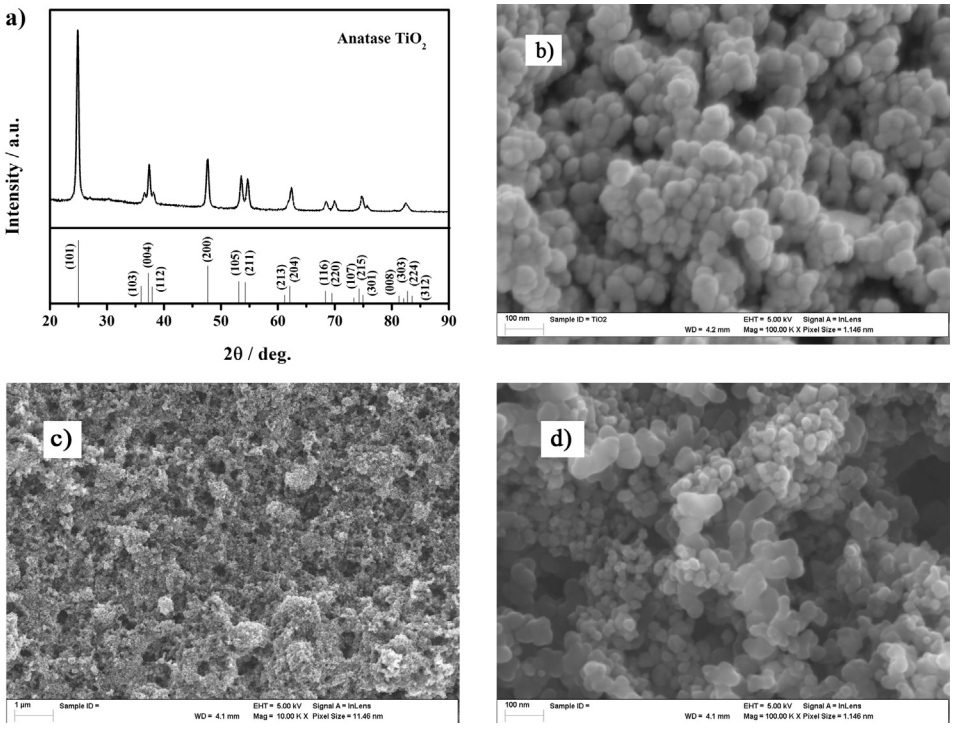

Fig. 1. Panel a) XRD pattern of TiO_2 nanoparticles; the reference for anatase TiO_2 (JCPDS card No. 00-021-1272) is shown in the bottom. Panel b) SEM image of TiO_2 nanoparticles at a magnification of 100 k×. Panels c) and d) SEM images of a pristine electrode at a magnification of 10 k× and 100 k×, respectively.

electrolyte compositions was investigated by means of galvanostatic cycling applying a specific current of 0.11C (≙36.9 mA g^{-1}) in a voltage window extending from 0.02 to 2.0 V (Fig. 2a).

The use of $NaPF_6$ results in the most stable cycling performance, however, at the expense of achievable specific capacity (only 120 mAh g^{-1} at the 20th cycle). The initial coulombic efficiency is rather low (42%), but then substantially increases to around 89% after 20 cycles. Cells comprising NaTFSI on the contrary present a significantly lower coulombic efficiency over the whole 20 cycles (except for the 1st cycle), reaching only 80% at the 20th cycle. The

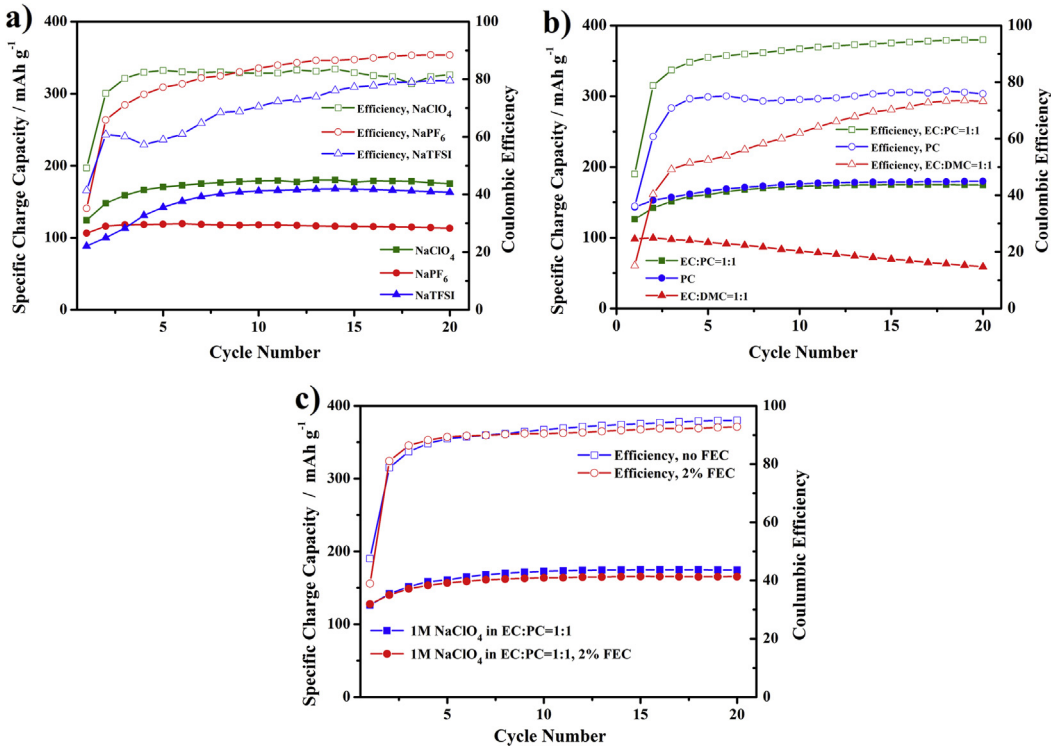

Fig. 2. Electrochemical performance of anatase TiO_2-based electrodes in terms of specific charge capacity (sodium release) *vs.* cycle number as a function of the sodium salt, using 1M NaX in PC (panel a), and the solvent, using 1M $NaClO_4$ electrolyte solutions (panel b). The effect of FEC as electrolyte additive in 1M $NaClO_4$ in EC:PC was also investigated (panel c). All cells were galvanostatically cycled at 0.11C (36.9 mA g^{-1}) setting the cut-off potentials to 0.02 and 2.0 V.

reversible specific capacity, however, although initially lower than for $NaPF_6$, increases to 158 mAh g^{-1} at the 10th cycle to finally stabilize at around 160 mAh g^{-1} in the following ones. Such an increase in specific capacity (even much more pronounced) was already reported for amorphous TiO_2 [34,35], possibly due to a relatively low initial adsorption of sodium ions to the TiO_2 surface [42]. Nevertheless, this point will be discussed later on again.

The highest specific capacity values were, indeed, obtained for $NaClO_4$, rising from initially 125 to 181 mAh g^{-1} after 20 cycles. This value is among the highest values reported so far for titanium-based sodium-ion anodes. Additionally, the coulombic efficiency is initially the highest among the three different electrolytes and rather stable after the second cycle, although surpassed by $NaPF_6$ after 10 cycles.

Based on these results $NaClO_4$ was chosen for the subsequent investigation of different electrolyte solvents (Fig. 2b). Organic carbonates, such as PC, ethylene carbonate (EC), dimethyl carbonate (DMC), and diethyl carbonate (DEC) are well known solvents for lithium- and sodium-ion batteries. Consequently, we prepared three different electrolyte compositions, 1M $NaClO_4$ in PC, 1M $NaClO_4$ in EC:DMC (1:1 by volume), and 1M $NaClO_4$ in EC:PC (1:1 by volume) for this survey. The mixture of EC and DEC was not investigated due to the poor solubility of $NaClO_4$ in it.

As immediately apparent from Fig. 2b, the TiO_2-based half-cell comprising EC:DMC as solvent shows the poorest performance in terms of achievable specific capacity, cycling stability, and coulombic efficiency. Such a half-cell shows an initial specific charge capacity of 100 mAh g^{-1} and a coulombic efficiency of 18% only. Moreover, after 20 cycles the capacity decreased to 80 mAh g^{-1}, while the coulombic efficiency did not exceed 71%. In fact, also Palacin and co-workers [41] observed low coulombic efficiencies for DMC-comprising electrolytes and assigned this to the decomposition of DMC at potentials lower than 1 V *vs.* Na/Na^+.

The comparison of those cells comprising PC and EC:PC reveals very similar results for the first cycle, *i.e.*, a reversible capacity of 125 mAh g^{-1} and a coulombic efficiency of 52%. Subsequently, both cells show increasing specific capacities and substantially enhanced coulombic efficiencies. Nonetheless, the coulombic efficiency for the cell employing the EC:PC mixture is substantially higher although its specific capacity is slightly lower than the one using only PC as solvent. After 20 cycles, the TiO_2-based electrode galvanostatically (dis-)charged using PC as electrolyte solvent showed a reversible capacity of 181 mAh g^{-1} and an efficiency of 82%, while the one cycled in EC:PC offered a capacity of 162 mAh g^{-1} and an efficiency of 94%. Palacin and co-workers [41] observed, indeed, similar results for their study on hard carbon-based electrodes. According to their results obtained by means of electrochemical impedance spectroscopy the mixture of EC and PC is able to form a stable SEI, while the SEI keeps continuously growing by using PC only. This issue will have to be investigated more in detail in future for anatase TiO_2-based electrodes. Nevertheless, with respect to the selected lower cut-off potential, these results are basically in very good agreement with the comparably lower coulombic efficiency observed for $NaClO_4$ in PC in Fig. 2b.

In fact, the results (Fig. 2a and b) are generally quite surprising, since $NaPF_6$ in PC (Fig. 2a) and $NaClO_4$ in EC:DMC (Fig. 2b) show the highest conductivity relatively to the other herein investigated electrolyte compositions [41], indicating that other factors must have a substantial influence on the reversible (de-)sodiation of anatase TiO_2. Presumably, the substantially improved performance of $NaClO_4$ in EC:PC electrolyte (Fig. 2b), additionally showing a solidification down to −120 °C as well as superior thermal and electrochemical stabilities [41], is linked to a beneficial chemical composition of the electrode/electrolyte interface. As previously mentioned already, this aspect deserves certainly further investigation by complementary techniques in future.

For the further investigation of nanoparticulate anatase TiO_2 as sodium-ion anode material we focused on the use of 1M $NaClO_4$ in EC:PC as electrolyte, since particularly a high coulombic efficiency

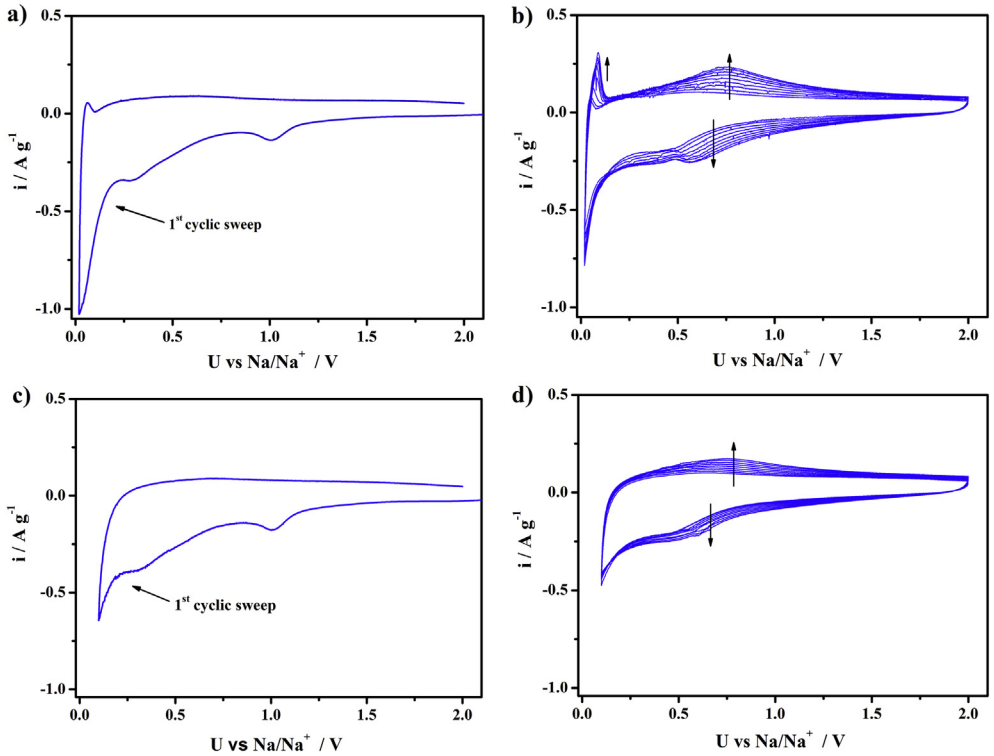

Fig. 3. Cyclic voltammograms of TiO_2-based electrodes at different reversing potentials: panels a) and b) 0.02 V & 2.0 V, panels c) and d) 0.1 V & 2.0 V *vs.* Na/Na^+. Panels a) and c) show the 1st cyclic sweep for each potential range, b) and d) present the subsequent nine (2nd to 10th) cyclic sweeps. Scan rate 0.5 mV s^{-1}.

is essential for the utilization of an active material in a sodium-ion-limited full-cell. According to Komaba et al. [43] the coulombic efficiency of some sodium-ion active materials could be further enhanced by adding a few percent of fluoroethylene carbonate (FEC) to the electrolyte. Hence, we studied also the influence of FEC on TiO_2-based electrodes (Fig. 2c). However, the performance is almost unaffected if not slightly worsened by the addition of FEC to the electrolyte. In fact, the 1st cycle reversibility is lower than for the pure electrolyte, and the coulombic efficiency and delivered specific capacity, initially very similar, become slightly inferior upon subsequent cycles. Previous studies on the utilization of FEC as electrolyte additive have shown contradictory results. While Komaba et al. [20,43] have reported a substantial improvement by adding FEC, Ponrouch et al. [19], for instance, have founddeleterious effects of FEC, *i.e.*, a reduced first cycle efficiency and an increased polarization, presumably resulting from a less conductive SEI.

Targeting further optimization of the coulombic efficiency, cyclic voltammetry was performed (Fig. 3). Setting the reversing potentials to 0.02 V and 2.0 V for the cathodic and anodic sweeps, respectively, reveals several characteristic features for the first cyclic sweep (Fig. 3a). The first cathodic peak at about 1 V was already observed for layered sodium titanates and assigned to electrolyte decomposition and SEI formation [44]. The origin of the rather broad peak at around 0.3 V is not fully clear, yet. Pan et al. [29] observed an irreversible peak at slightly higher potentials and assigned it to parasitic side reactions of the electrolyte. Nevertheless, with respect to the subsequent cyclic sweeps (Fig. 3b) it might also be that this peak does not disappear but shifts to higher potentials, possibly caused by a reduced overpotential for the reversible sodium ion storage. A similar effect, even if less pronounced, was indeed observed already for the reversible lithium insertion [45]. However, the third cathodic peak (Fig. 3a) close to reversing potential of 0.02 V is likely related to further electrolyte decomposition and a capacity contribution of the conductive carbon, as revealed by the anodic peak close to this potential, presumably related to the reversible sodium release [31,46,47]. While the specific current related to this phenomenon is apparently increasing upon cycling (Fig. 3b), being, in fact, in good agreement with the results reported by Rudola et al. [31], a new redox couple is continuously evolving at around 0.7 V (indicated by the arrows). The latter provides a reasonable explanation for the increasing specific capacity, as observed in Fig. 2. Obviously, the reversible sodiation of anatase TiO_2 is kinetically hampered and requires some kind of activation, for instance by an increased conductivity related to irreversible sodium trapping as reported for lithium [48]. This aspect certainly deserves further investigation and we are currently studying the underlying electrochemical processes in our lab. Indeed, very preliminary results indicate that sodium storage in anatase TiO_2 might follow a rather untypical mechanism. However, these results will be reported in a forthcoming communication. Concerning the increasing capacity contribution of the conductive carbon to the overall capacity, indicated by the increasing current intensity of the corresponding peak mentioned before, it can be assumed that this also results in an inferior coulombic efficiency, since the reactivity of sodiated carbonaceous materials in common organic carbonate-based electrolytes is rather high [18,49].

Thus, in order to further improve the coulombic efficiency for anatase TiO_2 upon continuous cycling, the cathodic reversing potential was increased from 0.02 to 0.1 V to prevent the uptake of sodium by the carbonaceous conductive additive (Fig. 3c and d). The first cyclic sweep (Fig. 3c) showed, in fact, the same characteristic features as before, simply the electrolyte decomposition at lower potentials close to 0 V and the sodium storage within the conductive carbon are significantly reduced if not fully inhibited regarding the latter. Indeed, no capacity contribution of the conductive carbon is observed for the subsequent anodic sweep. Upon further potentiodynamic cycling, however, the newly evolving redox couple becomes apparent (Fig. 3d), just as in the previous experiment (see again Fig. 3b).

3.3. Galvanostatic cycling and high rate performance

To further study the influence of the lower cut-off potential on the coulombic efficiency and in order to optimize the cycling procedure for anatase TiO_2-based electrodes, we performed a galvanostatic investigation increasing the sodiation cut-off potential for the first cycle from 0.02 V stepwise up to 0.3 V (Fig. 4). As expected, the discharge capacity decreases significantly by increasing the lower cut-off potential, presumably related to the lower extent of irreversible side reactions, including electrolyte decomposition (Fig. 4a). Interestingly, however, also the obtained reversible capacity upon charge (desodiation) decreases substantially by increasing the discharge cut-off potential from 0.02 V (126 mAh g^{-1}) to 0.2 V (48 mAh g^{-1}). Accordingly, the coulombic efficiency remains rather constant at about 50% independent of the lower cut-off value (Fig. 4a). Comparing the potential profiles for the corresponding charge steps reveals that the potential plateau observed for lower cut-offs vanishes continuously (Fig. 4b), indicating that some kind of activation of the active material is required initially.

Thus, considering all previous results, further electrochemical characterization of anatase TiO_2 nanoparticles by means of

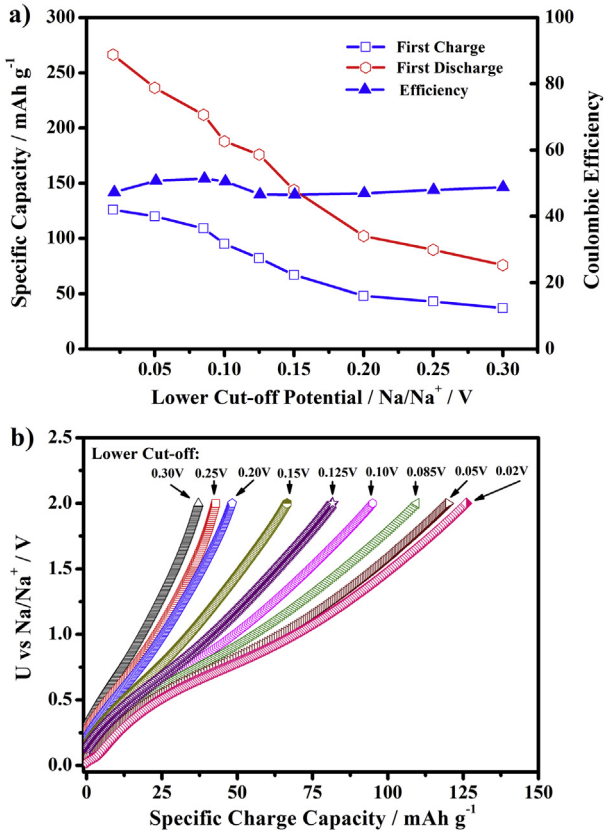

Fig. 4. Galvanostatic investigation of the influence of the lower cut-off potential on the coulombic efficiency for the first cycle: The upper cut-off potential is kept constant at 2.0 V, while the lower cut-off potential is set to 0.02 V, 0.05 V, 0.085 V, 0.10 V, 0.125 V, 0.15 V, 0.20 V, 0.25 V, and 0.30 V: a) the comparison of the thus obtained (dis-)charge capacities and the resulting coulombic efficiency relative to the lower cut-off potential; b) the corresponding potential profiles for the charge step.

galvanostatic cycling was performed using $NaClO_4$ in EC:PC as electrolyte (without FEC) and setting the cut-off potentials to 0.1 V and 2.0 V after performing two initial formation cycles using 0.02 V and 2.0 V as cut-off potentials. The performance and the voltage profile of a few selected cycles of TiO_2-based electrodes subjected to constant current cycling applying a C rate of 0.11C are reported in Fig. 5a and b, respectively. In accordance with the previous results the capacity is slightly increasing initially and stabilizes at about 145 mAh g^{-1} around the 20th cycle (Fig. 5a). After 60 cycles the specific capacity still amounts 135 mAh g^{-1} indicating a very reversible sodium ion uptake and release. The corresponding potential profiles for selected cycles (Fig. 5b) show that slight changes occurred upon cycling, revealing a more pronounced shape for the later cycles, which is in good agreement with the appearing redox couple as observed by cyclic voltammetry (Fig. 3). Most importantly, however, the coulombic efficiency finally exceeded 96%, which is a decent – nevertheless, certainly still improvable – value considering the impact of the sodium counter electrode on the overall efficiency.

In Fig. 5c and d, the rate capability of nanoparticulate anatase TiO_2-based electrodes is presented. After the electrode capacity had stabilized, increasing C rates were applied. As apparent from Fig. 5c, anatase TiO_2 nanoparticles show a superior high rate performance offering specific capacities of around 146, 134, 126, 115, 100, and 86 mAh g^{-1} at applied C rates of 0.22C, 0.55C, 1.1C, 2.2C, 5.5C, and 11C, respectively. It should be kept in mind that applied C rates of 5.5C and 11C correspond to specific currents as high as 1.85 and 3.69 A g^{-1}, respectively. To the best of our knowledge, such an advanced high rate performance, presumably *inter alia* supported by the porous morphology of the electrode coating layer (Fig. 1c and d), was never reported so far, neither for carbonaceous nor for titanium-based sodium-ion anodes. Remarkably moreover, by decreasing the C rate subsequently again to 0.11C, a specific capacity of more than 150 mAh g^{-1} was obtained, confirming the high reversibility of the sodiation process. In fact, this advanced rate capability is in good agreement with the theoretically predicted and experimentally confirmed diffusion barrier comparable to lithium ions [38]. Having a look at the corresponding potential

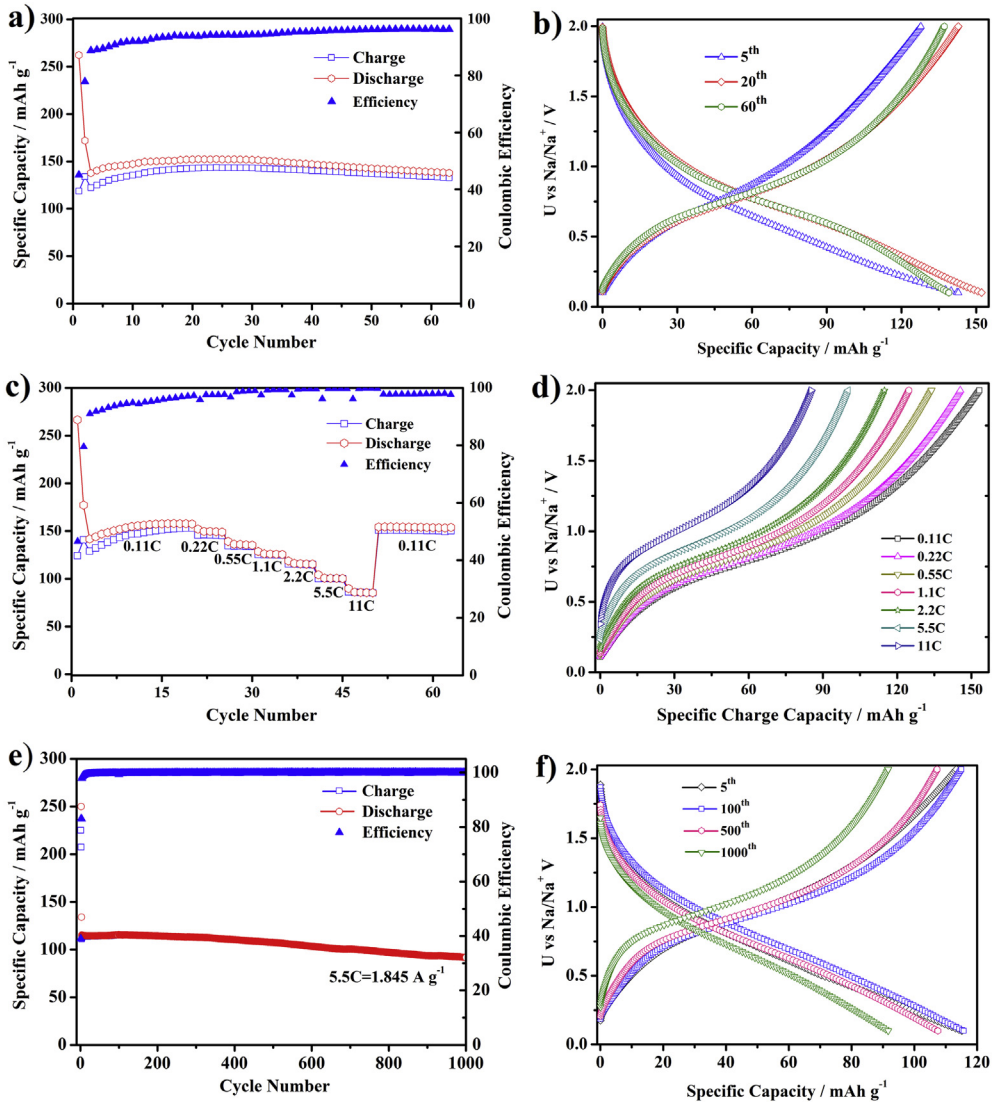

Fig. 5. a) Galvanostatic cycling at 0.11C (36.9 mA g^{-1}) of a TiO_2 half-cell using a mixture of 1M $NaClO_4$ in EC:PC (1:1 by volume) as electrolyte; cut-off potentials: 0.1 V and 2.0 V (after two formation cycles using 0.02 V and 2.0 V as cut-off potentials). b) Corresponding potential profiles for selected cycles (*i.e.*, the 5th, 20th, and 60th cycle). c) Galvanostatic cycling at elevated C rates after stabilization at 0.11C (≙36.9 mA g^{-1}); each 5 cycles at 0.22, 0.55, 1.1, 2.2, 5.5, and 11C (1C ≙369 mA g^{-1}). d) Corresponding potential profiles for selected cycles at different C rates (*i.e.*, the 20th, 25th, 30th, 35th, 40th, 45th, and 50th cycle at 0.11, 0.22, 0.55, 1.1, 2.2, 5.5, and 11C, respectively); for clarity reasons only the charge steps are shown in panel d). e) Galvanostatic cycling at 5.5C (≙1.845 A g^{-1}). f) Corresponding potential profiles for selected cycles (*i.e.*, the 5th, 100th, 500th, and 1000th cycle).

profiles for selected charge steps (Fig. 5d), it is obvious that the characteristic potential profile is preserved for all C rates up to 11C and that the slight capacity decrease for elevated C rates is basically related to an increasing polarization, particularly for the highest applied C rates (5.5C and 11C).

Finally, the long-term cycling stability at such elevated specific currents was studied (Fig. 5e and f). Electrodes were galvanostatically cycled at 5.5C, presenting a stable performance for more than 1000 cycles without substantial capacity loss upon cycling (Fig. 5e, 92 mAh g^{-1} for the 1000th cycle), revealing once again the highly reversible sodium-ion uptake and release. However, comparing the corresponding potential profiles for the 100th and 500th cycle (Fig. 5f) reveals that the initial slight capacity decay after about 350 cycles is basically related to a shortening of the voltage plateau. Upon continuous cycling an increasing internal resistance (*i.e.*, an increasing polarization for the charge and discharge step comparing the 500th and 1000th cycle) appears to lead to a further decrease in capacity. Particularly regarding the latter, a continuing optimization of the electrolyte composition, for instance, by identifying suitable additives, might enable further improvement of the long-term cycling stability. Nevertheless, it should be kept in mind that the herein presented capacity retention of about 82% after 1000 cycles at 5.5C using half-cell configuration are certainly already highly promising with respect to the future application of anatase TiO_2 nanoparticles in high-power sodium-ion batteries.

4. Conclusions

Anatase TiO_2 nanoparticles were electrochemically characterized as sodium-ion anode material. Various electrolyte compositions (different salts and solvents) were studied. The best performance in terms of achievable specific capacity, cycling stability, and coulombic efficiency, was obtained by using $NaClO_4$ as conducting salt in an EC:PC solvent mixture. The coulombic efficiency was further improved by increasing the cathodic cut-off potential to 0.1 V, thus preventing the partially irreversible capacity contribution of the conductive carbon, while FEC as electrolyte additive did not show any improvement.

More remarkably however, electrodes based on nanoparticulate anatase TiO_2 and CMC as binder showed an advanced high rate capability, offering specific capacities of around 100 and 86 mAh g^{-1} at 5.5C and 11C, *i.e.,* an applied specific current of about 1.85 and 3.69 A g^{-1}, respectively. Moreover, setting the C rate to 5.5C, such electrodes present a very stable cycling performance for more than 1000 cycles without significant capacity decay. Based on these results anatase TiO_2 nanoparticles appear as a highly promising, environmentally benign, and cost-efficient candidate for sodium-ion anodes, particularly for high-power applications.

Acknowledgment

Liming Wu would like to acknowledge the Chinese Scholarship Council for financial support.

References

[1] J.M. Tarascon, M. Armand, Nature 414 (2001) 359–367.
[2] J.B. Goodenough, Y. Kim, J. Power Sources 196 (2011) 6688–6694.
[3] B. Scrosati, J. Hassoun, Y.-K. Sun, Energy Environ. Sci. 4 (2011) 3287–3295.
[4] M. Armand, J.M. Tarascon, Nature 451 (2008) 652–657.
[5] J.-M. Tarascon, Nat. Chem. 2 (2010) 510.
[6] C. Wadia, P. Albertus, V. Srinivasan, J. Power Sources 196 (2011) 1593–1598.
[7] V. Palomares, P. Serras, I. Villaluenga, K.B. Hueso, J. Carretero-Gonzalez, T. Rojo, Energy Environ. Sci. 5 (2012) 5884–5901.
[8] K. Sung-Wook, S. Dong-Hwa, M. Xiaohua, G. Ceder, K. Kisuk, Adv. Energy Mater. 2 (2012) 710–721.
[9] B.L. Ellis, L.F. Nazar, Curr. Opin. Solid State Mater. Sci. 16 (2012) 168–177.
[10] M.D. Slater, D. Kim, E. Lee, C.S. Johnson, Adv. Funct. Mater. 23 (2013) 947–958.
[11] L. Zhonghua, J.R. Dahn, J. Electrochem. Soc. 148 (2001) A1225–A1229.
[12] R. Berthelot, D. Carlier, C. Delmas, Nat. Mater. 10 (2011) 74–80.
[13] D. Buchholz, A. Moretti, R. Kloepsch, S. Nowak, V. Siozios, M. Winter, S. Passerini, Chem. Mater. 25 (2013) 142–148.
[14] Y. Kawabe, N. Yabuuchi, M. Kajiyama, N. Fukuhara, T. Inamasu, R. Okuyama, I. Nakai, S. Komaba, Electrochemistry 80 (2012) 80–84.
[15] A.K. Padhi, K.S. Nanjundaswamy, C. Masquelier, J.B. Goodenough, J. Electrochem. Soc. 144 (1997) 2581–2586.
[16] Z. Jian, W. Han, X. Lu, H. Yang, Y.-S. Hu, J. Zhou, Z. Zhou, J. Li, W. Chen, D. Chen, L. Chen, Adv. Energy Mater. 3 (2013) 156–160.
[17] D.A. Stevens, J.R. Dahn, J. Electrochem. Soc. 148 (2001) A803–A811.
[18] R. Alcantara, P. Lavela, G.F. Ortiz, J.L. Tirado, R. Menendez, R. Santamaria, J.M. Jimenez-Mateos, Carbon 41 (2003) 3003–3013.
[19] A. Ponrouch, A.R. Goni, M. Rosa Palacin, Electrochem. Commun. 27 (2013) 85–88.
[20] S. Komaba, W. Murata, T. Ishikawa, N. Yabuuchi, T. Ozeki, T. Nakayama, A. Ogata, K. Gotoh, K. Fujiwara, Adv. Funct. Mater. 21 (2011) 3859–3867.
[21] S.-M. Oh, S.-T. Myung, M.-W. Jang, B. Scrosati, J. Hassoun, Y.-K. Sun, Phys. Chem. Chem. Phys. 15 (2013) 3827–3833.
[22] L.D. Ellis, T.D. Hatchard, M.N. Obrovac, J. Electrochem. Soc. 159 (2012) A1801–A1805.
[23] L. Baggetto, P. Ganesh, R.P. Meisner, R.R. Unocic, J.-C. Jumas, C.A. Bridges, G.M. Veith, J. Power Sources 234 (2013) 48–59.
[24] D.-J. Lee, J.-W. Park, I. Hasa, Y.-K. Sun, B. Scrosati, J. Hassoun, J. Mater. Chem. A 1 (2013) 5256–5261.
[25] D. Bresser, F. Mueller, D. Buchholz, E. Paillard, S. Passerini, Electrochim. Acta, http://dx.doi.org/10.1016/j.electacta.2013.09.007.
[26] Y.-M. Lin, P.R. Abel, A. Gupta, J.B. Goodenough, A. Heller, C.B. Mullins, ACS Appl. Mater. Interfaces 5 (2013) 8273–8277.
[27] L. Wu, X. Hu, J. Qian, F. Pei, F. Wu, R. Mao, X. Ai, H.X. Yang, Y. Cao, Energy Environ. Sci. (2013), http://dx.doi.org/10.1039/C3EE42944J.
[28] J. Fullenwarth, A. Darwiche, A. Soares, B. Donnadieu, L. Monconduit, J. Mater. Chem. A, http://dx.doi.org/10.1039/c3ta13976j.
[29] H. Pan, X. Lu, X. Yu, Y.-S. Hu, H. Li, X.-Q. Yang, L. Chen, Adv. Energy Mater. 9 (2013) 1186–1194.
[30] P. Senguttuvan, G. Rousse, V. Seznec, J.-M. Tarascon, M. Rosa Palacin, Chem. Mater. 23 (2011) 4109–4111.
[31] A. Rudola, K. Saravanan, C.W. Mason, P. Balaya, J. Mater. Chem. A 1 (2013) 2653–2662.
[32] W. Wang, C. Yu, Y. Liu, J. Hou, H. Zhu, S. Jiao, RSC Adv. 3 (2013) 1041–1044.
[33] J.P. Huang, D.D. Yuan, H.Z. Zhang, Y.L. Cao, G.R. Li, H.X. Yang, X.P. Gao, RSC Adv. 3 (2013) 12593–12597.
[34] H. Xiong, M.D. Slater, M. Balasubramanian, C.S. Johnson, T. Rajh, J. Phys. Chem. Lett. 2 (2011) 2560–2565.
[35] Z. Bi, M.P. Paranthaman, P.A. Menchhofer, R.R. Dehoff, C.A. Bridges, M. Chi, B. Guo, X.-G. Sun, S. Dai, J. Power Sources 222 (2013) 461–466.
[36] J.R. González, R. Alcántara, G.F. Ortiz, F. Nacimiento, J.L. Tirado, J. Electrochem. Soc. 160 (2013) A1390–A1398.
[37] L. Kavan, K. Kratochvilova, M. Grätzel, J. Electroanal. Chem. 394 (1995) 93–102.
[38] S. Lunell, A. Stashans, L. Ojamae, H. Lindstrom, A. Hagfeldt, J. Am. Chem. Soc. 119 (1997) 7374–7380.
[39] Y. Xu, E. Memarzadeh Lotfabad, H. Wang, B. Farbod, Z. Xu, A. Kohandehghan, D. Mitlin, Chem. Commun. 49 (2013) 8973–8975.
[40] K. Xu, Chem. Rev. 104 (2004) 4303–4417.
[41] A. Ponrouch, E. Marchante, M. Courty, J.-M. Tarascon, M.R. Palacin, Energy Environ. Sci. 5 (2012) 8572–8583.
[42] B. Enright, G. Redmond, D. Fitzmaurice, J. Phys. Chem. 98 (1994) 6195–6200.
[43] S. Komaba, T. Ishikawa, N. Yabuuchi, W. Murata, A. Ito, Y. Ohsawa, ACS Appl. Mater. Interfaces 3 (2011) 4165–4168.
[44] M. Shirpour, J. Cabana, M. Doeff, Energy Environ. Sci. 6 (2013) 2538–2547.
[45] D. Bresser, E. Paillard, E. Binetti, S. Krueger, M. Striccoli, M. Winter, S. Passerini, J. Power Sources 206 (2012) 301–309.
[46] D.A. Stevens, J.R. Dahn, J. Electrochem. Soc. 147 (2000) 4428–4431.
[47] R. Alcantara, P. Lavela, G.F. Ortiz, J.L. Tirado, Electrochem. Solid State Lett. 8 (2005) A222–A225.
[48] R. van de Krol, A. Goossens, J. Schoonman, J. Phys. Chem. B. 103 (1999) 7151–7159.
[49] X. Xia, J.R. Dahn, J. Electrochem. Soc. 159 (2012) A515–A519.